Exciton-Condensate-Like Amplification of Energy Transport in Light Harvesting

Anna O. Schouten, LeeAnn M. Sager-Smith, and David A. Mazziotti*
Department of Chemistry and The James Franck Institute,
The University of Chicago, Chicago, IL 60637 USA
(Dated: Submitted December 21, 2022; Revised March 11, 2023)

* damazz@uchicago.edu

I. BASIS EQUIVALENCE

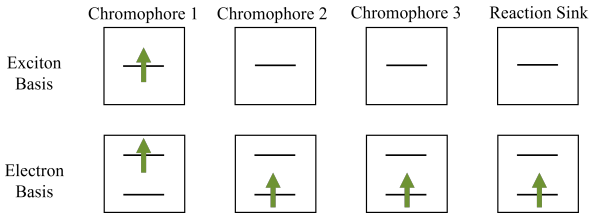

FIG. S1: Pictorial description of the basis mapping from the exciton basis (top) to the electron basis (bottom). In the exciton basis, the arrow represents an exciton occupying the orbital. In the electron basis, each arrow represents an electron and the electron in an upper level indicates it has been excited to form an exciton. The two representations shown demonstrate the initial excitation of the density matrix and are equivalent in their respective bases.

II. 7 CHROMOPHORES

Fig. S2 shows population and λ_G dynamics for the entangled model with all seven chromophores, V = 0.6, and two sites per chromophore. Fig. S3 shows population and λ_G dynamics for the localized model with all seven chromophores, V = 0.6, and two sites per chromophores. Although the rate of transfer is reduced relative to the the three chromophore subsystem, the full seven chromophore dynamics are generally similar to those of the three chromophore subsystem. Thus, our use of the three chromophore subsystem throughout the main text seems reasonable.

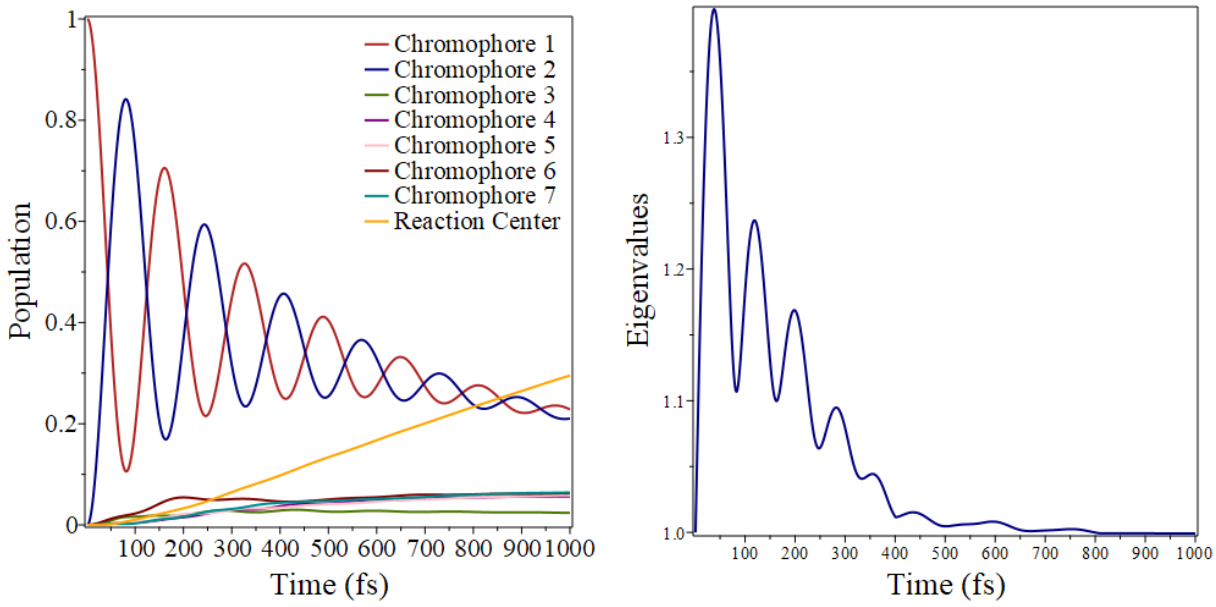

(a) Populations

(b) Eigenvalues

FIG. S2: Seven chromophore model for two sites per chromophore with the entangled initial excitation and V = 0.6.

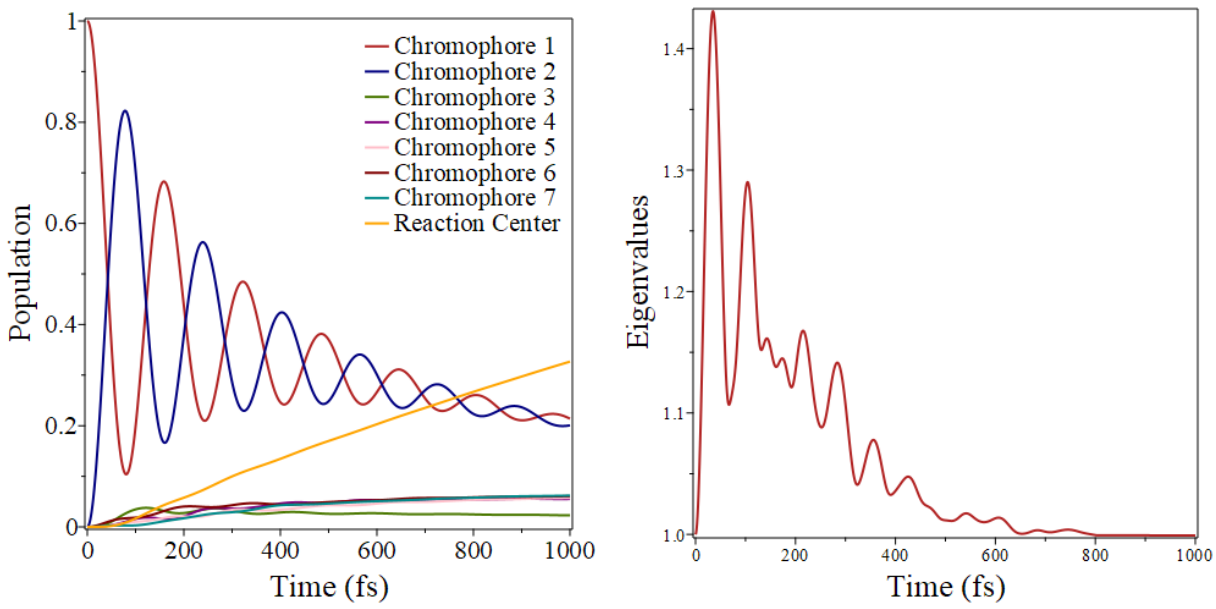

(a) Populations (b) Eigenvalues

FIG. S3: Seven chromophore model for two sites per chromophore with the localized initial excitation and V = 0.6.

III. $\xi > 0$

Fig. S4 shows comparisons of the reaction center population with varying values of V for the entangled model with two sites per chromophore and Fig. S5 shows the same for the localized model. In all cases, the most efficicent transfer occurs when $\xi = 0$. This is the result of destructive interference, similar to the differences with variation in the value of V (see below), which is greater when the cross-site inter-chromophore coupling and within-site inter-chromophore coupling are more balanced. Destructive interference is reduced when only one type of inter-chromophore coupling is present and is least for inclusion of only within-site inter-chromophore coupling. Therefore, all results in the main text are presented exclusively for $\xi = 0$.

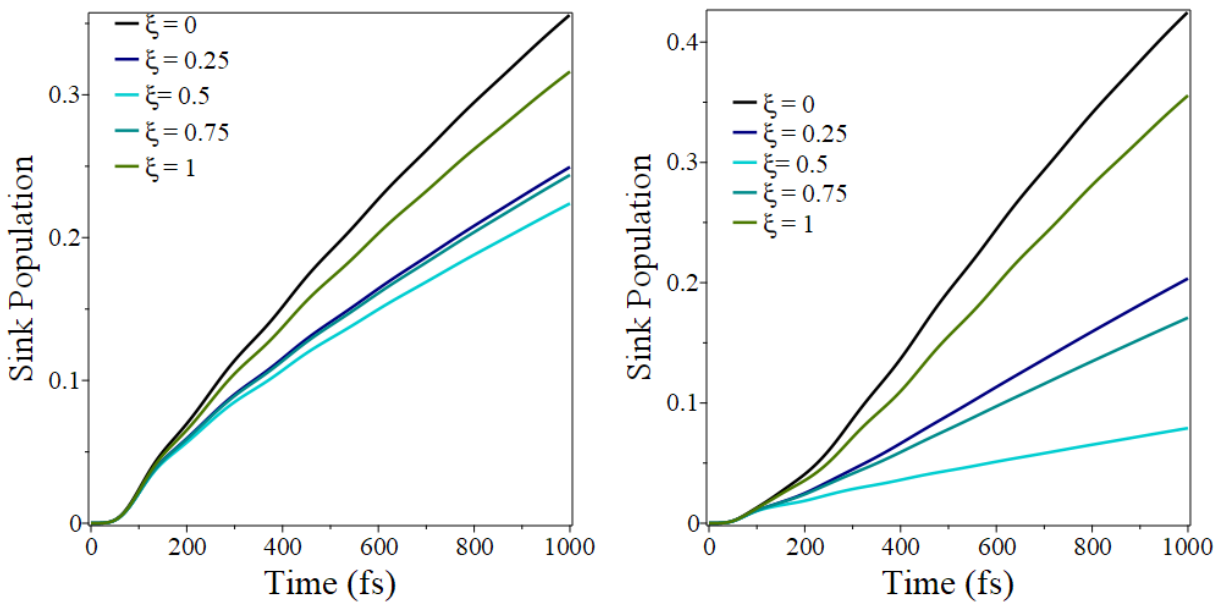

(a) V = 0 (b) V = 0.6

FIG. S4: Comparison of reaction center population for varying values of ξ for the entangled model with two sites per chromophore.

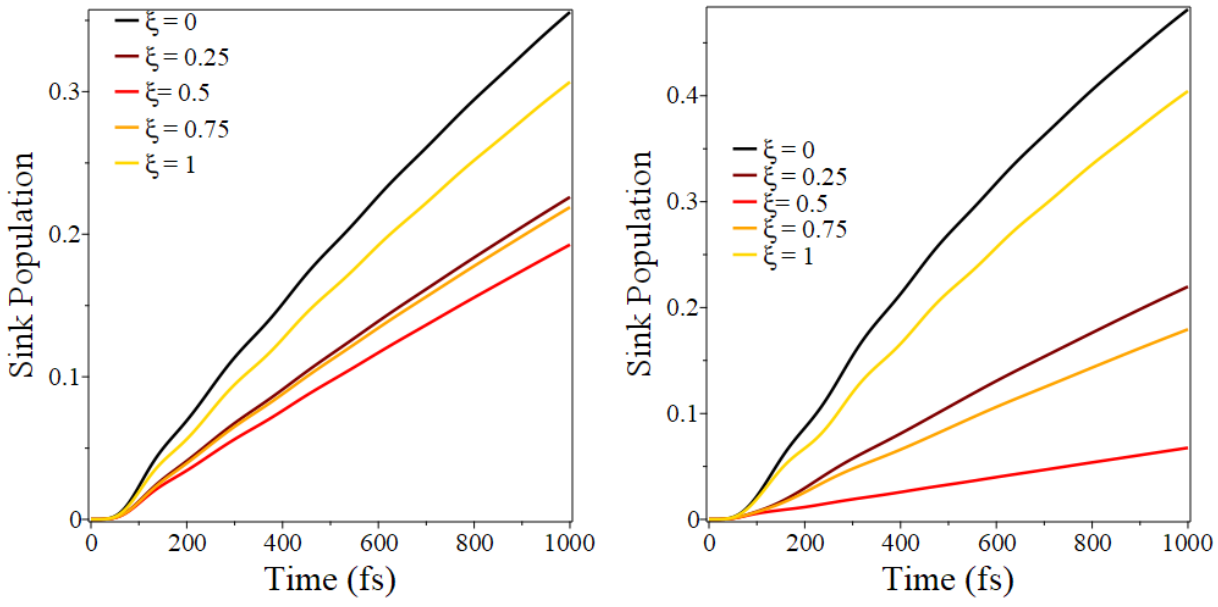

(a) V = 0 (b) V = 0.6

FIG. S5: Comparison of reaction center population for varying values of ξ for the localized model with two sites per chromophore.

Fig. S6 shows the λ_G dynamics of the entangled initial excitation for $M = 2$ with $V = 0$ and $V = 0.6$ for varying values of ξ. Fig. S7 show the same for the localized initial excitation. The results demonstrate that despite the reduction in exciton transfer, the large eigenvalue in connection with the population dynamics occurs when the sites on the same chromophore can interact.

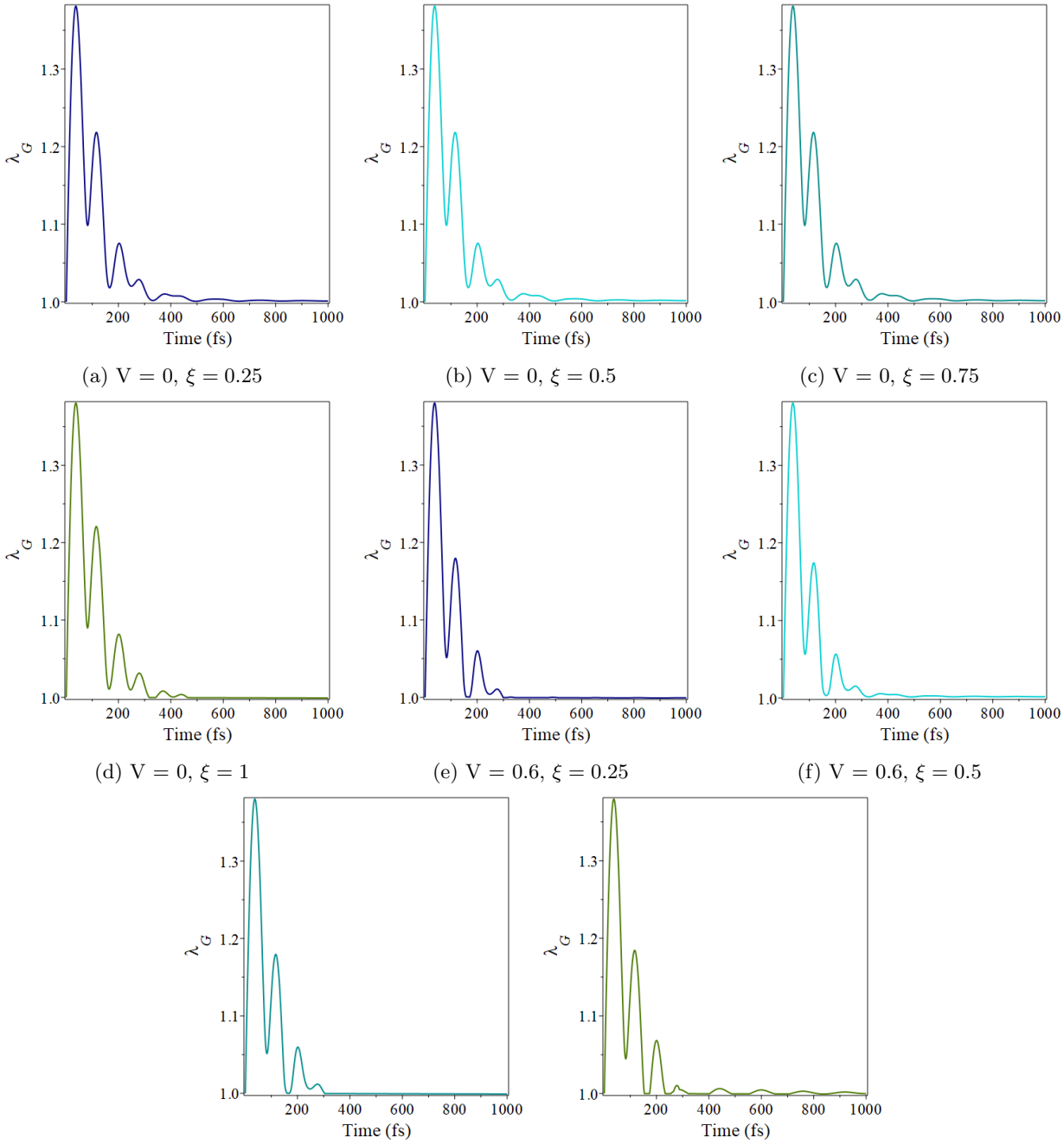

(a) V = 0, $\xi = 0.25$ (b) V = 0, $\xi = 0.5$ (c) V = 0, $\xi = 0.75$

(d) V = 0, $\xi = 1$ (e) V = 0.6, $\xi = 0.25$ (f) V = 0.6, $\xi = 0.5$

(g) V = 0.6, $\xi = 0.75$ (h) V = 0.6, $\xi = 1$

FIG. S6: λ_G dynamics for entangled initial excitation with varying values of ξ.

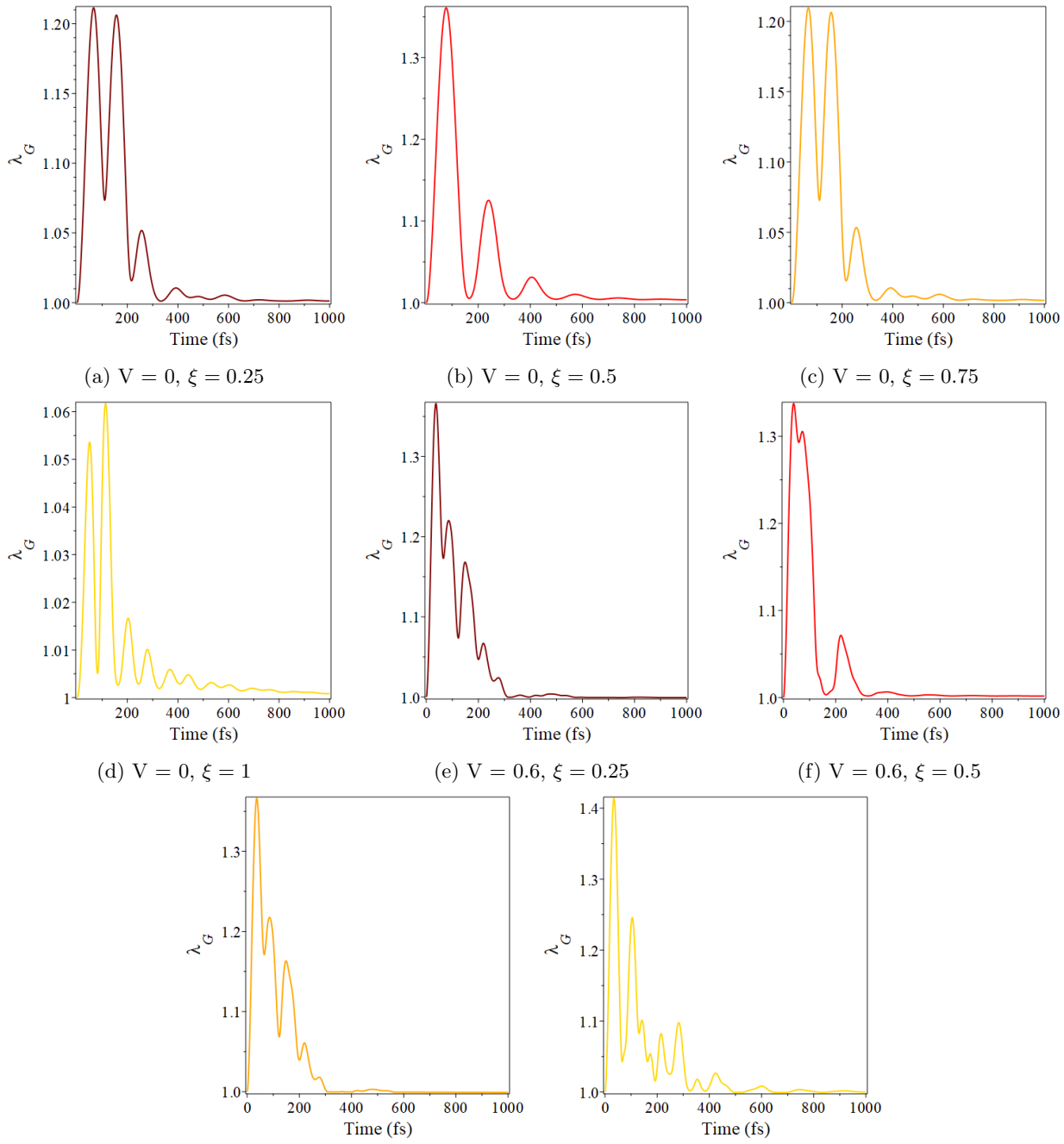

(a) V = 0, $\xi = 0.25$ (b) V = 0, $\xi = 0.5$ (c) V = 0, $\xi = 0.75$

(d) V = 0, $\xi = 1$ (e) V = 0.6, $\xi = 0.25$ (f) V = 0.6, $\xi = 0.5$

(g) V = 0.6, $\xi = 0.75$ (h) V = 0.6, $\xi = 1$

FIG. S7: λ_G dynamics for localized initial excitation with varying values of ξ.

IV. WITHOUT DEPHASING

Dephasing is added to the dynamics by the Lindbladian operator and has been previously identified to assist in exciton transfer by suppressing destructive interference [1]. As described in the main text, when dephasing is removed transfer of excitons to the reaction center is greatly reduced and the exciton population is trapped in oscillations between chromphores 1 and 2. This is particularly notable in the entangled model (Fig. S8a) where around 95% of the population remains trapped between these two chromophores even after 1000 fs. When the population is not transferred to the sink and remains trapped between these two chromophores, the value of λ_G is large and does not decay as in other cases (Fig. S8b), suggesting that the entanglement leading to the large eigenvalue is primarily

entanglement between chromophores 1 and 2. The same patterns are evident for the localized model (Fig. S9), however, greater transfer of exciton population to the reaction center occurs. In fact, after 1000 fs, only around 67% of the exciton population remains in chromophores 1 and 2 and some decay of the large eigenvalue occurs. This may be due to the interference patterns in the populations of the individual sites of the chromophores, which could help reduce destructive interference even in the absence of dephasing.

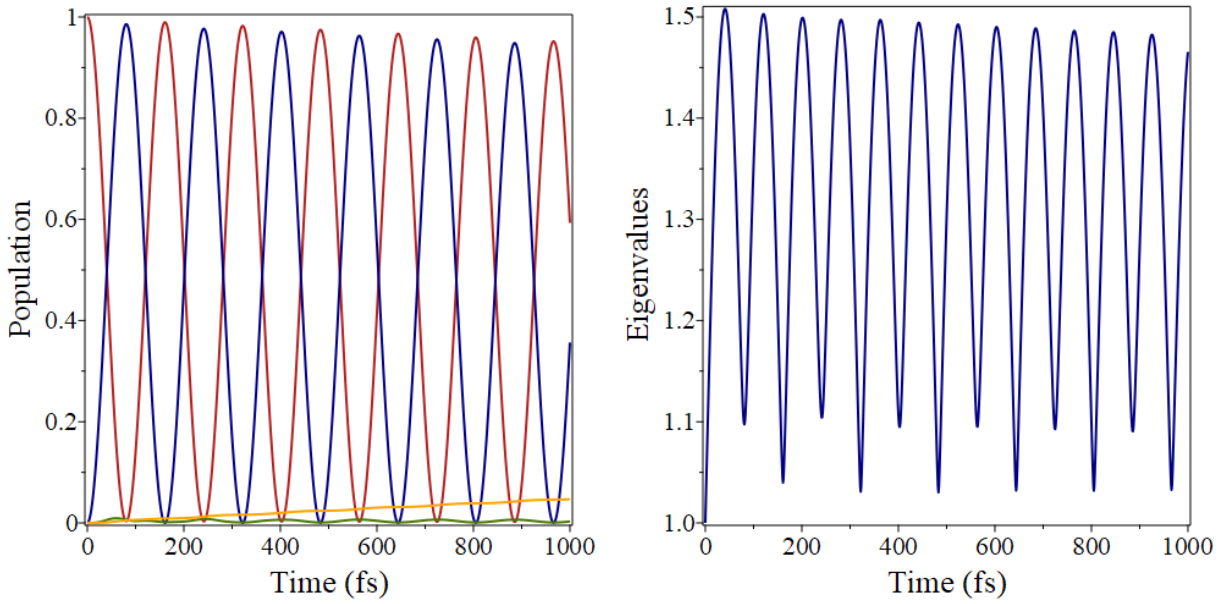

(a) Populations (b) Eigenvalues

FIG. S8: Entangled model with two sites per chromophore, V = 0.6, and no dephasing.

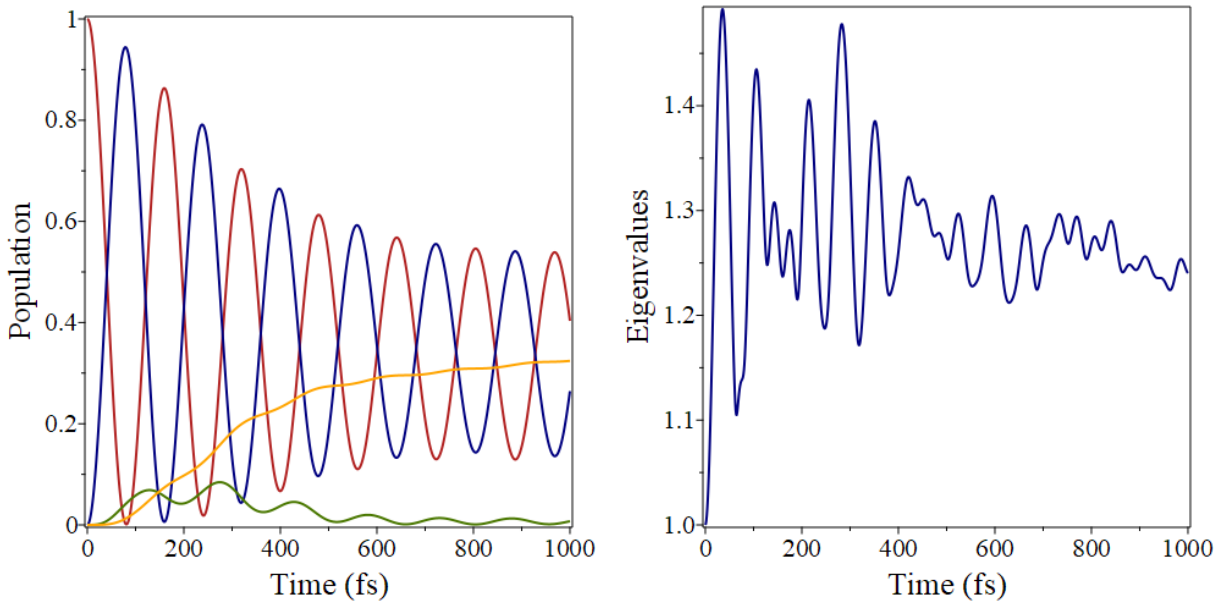

(a) Populations (b) Eigenvalues

FIG. S9: Localized model with two sites per chromophore, V = 0.6, and no dephasing.

V. QUANTUM INTERFERENCE

The differences in transfer rate with different values of V results from quantum interference introduced by intra-chromophore coupling which can be either constructive, leading to increased transfer rates, or destructive, leading to reduced transfer rates. While this is true in the both the entangled and localized models, in the localized model the signature of the interference can also be seen in the differences of the populations of the sites on individual chromphores. Because the localized model initially excites a single site on chromophore 1, there is one site that is populated differently throughout the simulation. Fig. S10 shows the populations of the two sites on chromophore 1 for the localized model with two sites per chromophore and the interference patterns for the various values of V shoe interference patterns in the populations of the two sites. In this case, the plots show that for $V = 0.6$, which has the greatest transfer, the interference is mostly constructive, in constrast to $V = 1$ which has the least transfer, where the interference is mostly destructive. Similar destructive interference is present for values of $\xi > 0$ which leads to reduced transfer. It is worth noting that the interference in the populations is the *result* of the quantum interference leading to differences in transfer rather than the *cause*, as in the entangled model, such interference in the populations can not be observed but the rate of transfer is still affected.

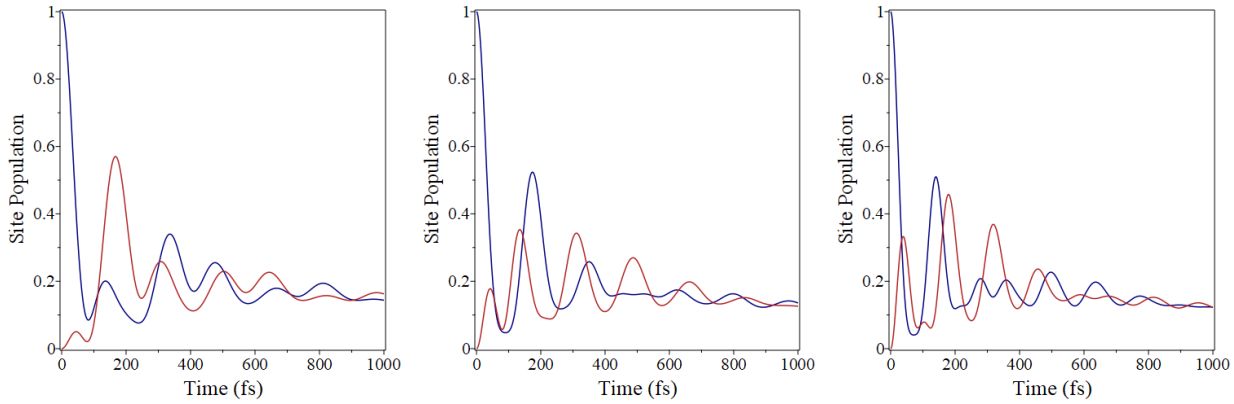

(a) V = 0.2 (b) V = 0.4 (c) V = 0.6

(d) V = 0.8 (e) V = 1

FIG. S10: Interference patterns in the populations of chromophore 1 for the localized model with two sites per chromophore. The navy line is the excited site in the initial timestep and the red line is the site without an excitation in the initial timestep.

VI. TRANSFER RATES WITH DIFFERENT VALUES OF V

The rates of transfer to the reaction center—calculated as finite differences in the reaction center population—are shown in Figs. S11b and S11a. For the entangled model, the rates show that $V = 0$, or the case with no intra-chromophore coupling, initially has the largest rate of transfer. This initially large rate of transfer quickly decays and the rates of transfer for $V = 0.2,\ 0.4,\ 0.6$, and 0.8 peak in the region of 300-400 fs such that all except $V = 0.8$, which

has a much slower initial rate of transfer, have greater final exciton populations than $V = 0$. The rate of transfer for $V = 1$ remains lower than that of $V = 0$ for much of the simulation, resulting in reduced overall transfer. In contrast to the entangled model, where the rates of transfer for the coupled model are initially slow and peak after that of $V = 0$, the rates for the localized model more closely follow the pattern of the uncoupled (or $V = 0$) rate. For all values of V, the rates have a peak in the region of 100-200 fs, which then decays for $V = 0$, 0.2, 0.8, and 1, but leads to another large peak for $V = 0.4$ and 0.6. Interestingly, $V = 0.8$ and 1 have the largest rates initially, but the rate rapidly decays to result in less transfer, whereas $V = 0.4$ and 0.6 have lower initial rates but then increase and eventually decay more slowly. The localized model results in generally higher rates of transfer than the entangled model, despite the fact that the two models have identical rates of transfer in the uncoupled case. The dampening effect of destructive interference could help explain why in the localized model the rates of $V = 1$ and $V = 0.8$ are slower overall, despite initially high rates.

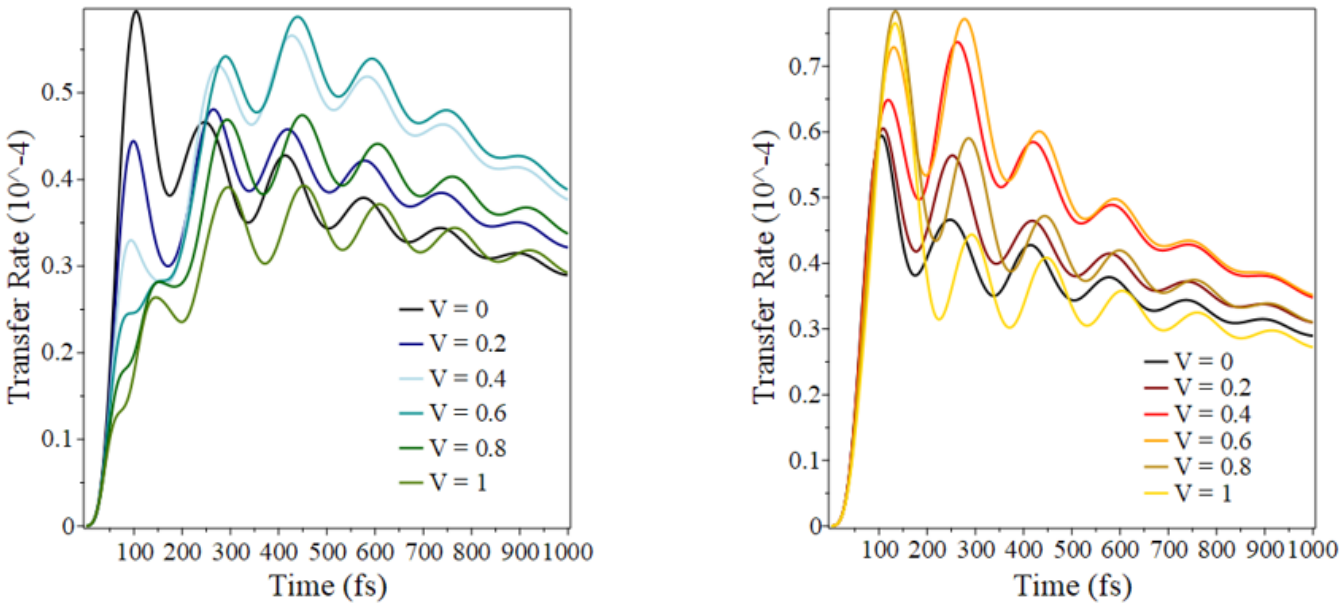

(a) Entangled initial excitation

(b) Localized initial excitation

FIG. S11: Transfer rates with varying values of V.

VII. TRANSFER RATES WITH INCREASING VALUES OF M

By comparing the exciton transfer rates for increasing values of M in Figs. S12a and S12b, we see that as before, the localized model has generally higher transfer rates. For the entangled model, the uncoupled model (one site) again has a higher initial transfer rate relative to any number of sites. Notably, the shape of the transfer rate spectra for the uncoupled and two site cases do not follow the same pattern as the rates of larger numbers of sites. The cases for four, six, ten, and 20 sites per chromophore all follow a pattern of slow growth in transfer rate, with a narrow shelf around 100-200 fs, reaching a maximum in the region of 400-500 fs before rapidly decaying. However, with two sites, the shelf prior to the maximum peak is broader and the decay after the largest peak is much less steep. The uncoupled case follows a different path, reaching a peak around 100 fs and decaying for the remainder of the simulation. The differences may be related to the nature of the entangled starting state. A minimum of three particles is required for condensation of excitons [2, 3], meaning that while the four, six, ten, and 20 site cases would have the potential for such condensation in the starting state, neither the uncoupled nor the two site case could exhibit such entanglement. This difference could influence the pattern of the way that excitons are transferred in this model and will be further discussed in a subsequent section.

In contrast to the differences in the shapes of the rate plots for the entangled model, the pattern of the transfer rate for the localized model is fairly consistent for more than one site per chromophore. The plots of the transfer rates each show a large peak in the rate near 100 fs followed by a second peak of similar magnitude around 250-300 fs before a rapid decay in rate starting around 400-500 fs, particularly for greater numbers of sites, with the rates of the 20, ten, six, and four site cases approaching convergence with that of the two site case near 1000 fs. While

the initial rates are greater for larger numbers of sites, the overall trend of the rates generally follows that of the uncoupled model. This suggests that the nature of exciton transfer for the localized model may resemble the uncoupled model more closely than does the entangled model. However, both models maintain the same spectral structure in the population dynamics, meaning that the exciton population is still passed between chromophores 1 and 2 in a oscillatory manner before transferring to chromophore 3 and finally the reaction center. Additionally, the frequency of the oscillations between the populations of chromophores 1 and 2 remain approximately the same, independent of the starting excitation model, the value of V, and the number of sites per chromophore.

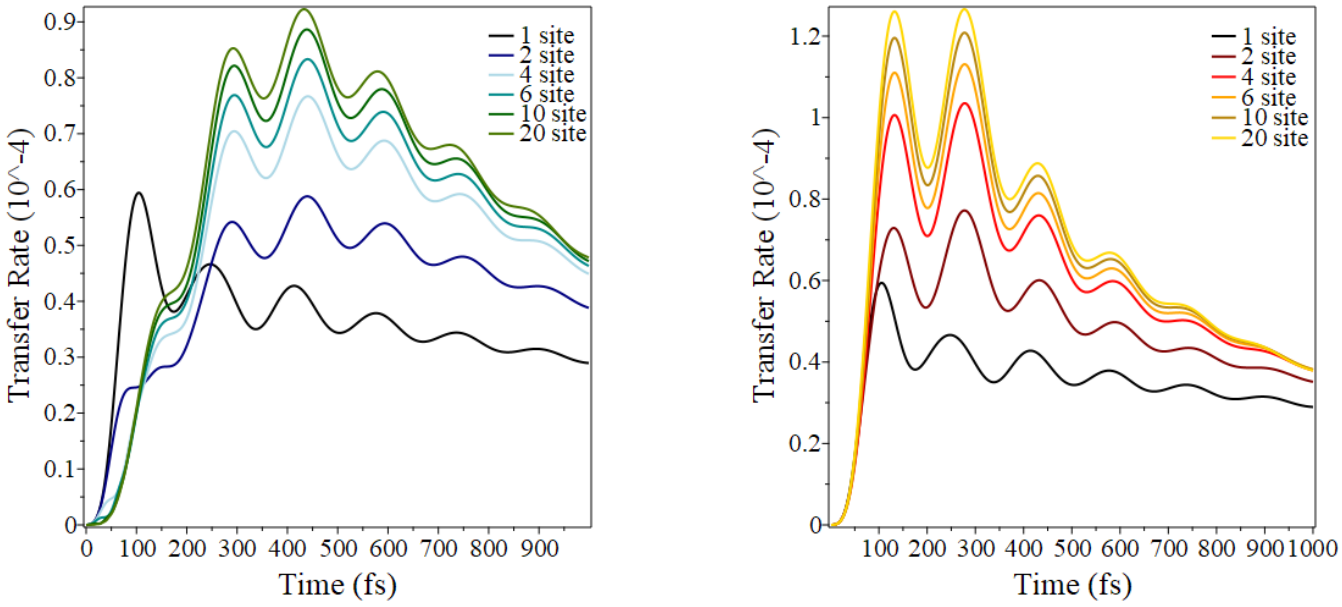

(a) Entangled initial excitation

(b) Localized initial excitation

FIG. S12: Transfer rates with varying values of M.

VIII. λ_G DYNAMICS WITH DIFFERENT VALUES OF V

Fig. S13 shows plots of the λ_G dynamics for the entangled model with two sites per chromophore and Fig. S14 shows the same for the localized model. For the entangled model, the shape of the spectra are fairly independent of the value of V, but greater values of V appear to have longer coherence times. For the localized model, the general decay pattern is the same regardless of the value of V, but larger values of V appear to have greater peak frequency and longer coherence time. The peak increase in peak frequency may be the result of more frequent exchange of populations between sites of the same chromophore, as the same increase in frequency appears in the interference patterns of the site populations (Fig. S10). This could also contribute to the longer coherence times we observe for both the entangled and localized models.

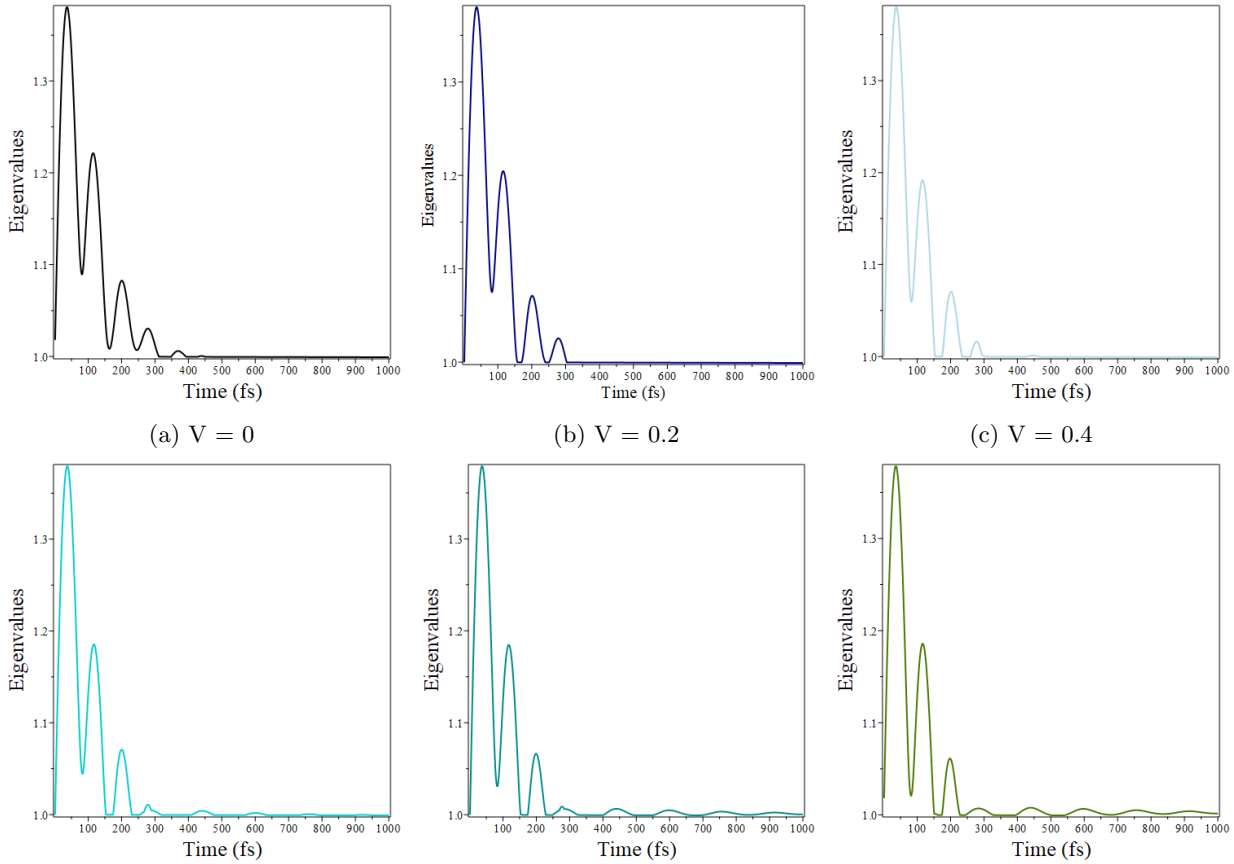

(a) V = 0 (b) V = 0.2 (c) V = 0.4

(d) V = 0.6 (e) V = 0.8 (f) V = 1

FIG. S13: λ_G Dynamics for entangled model with two sites per chromophore.

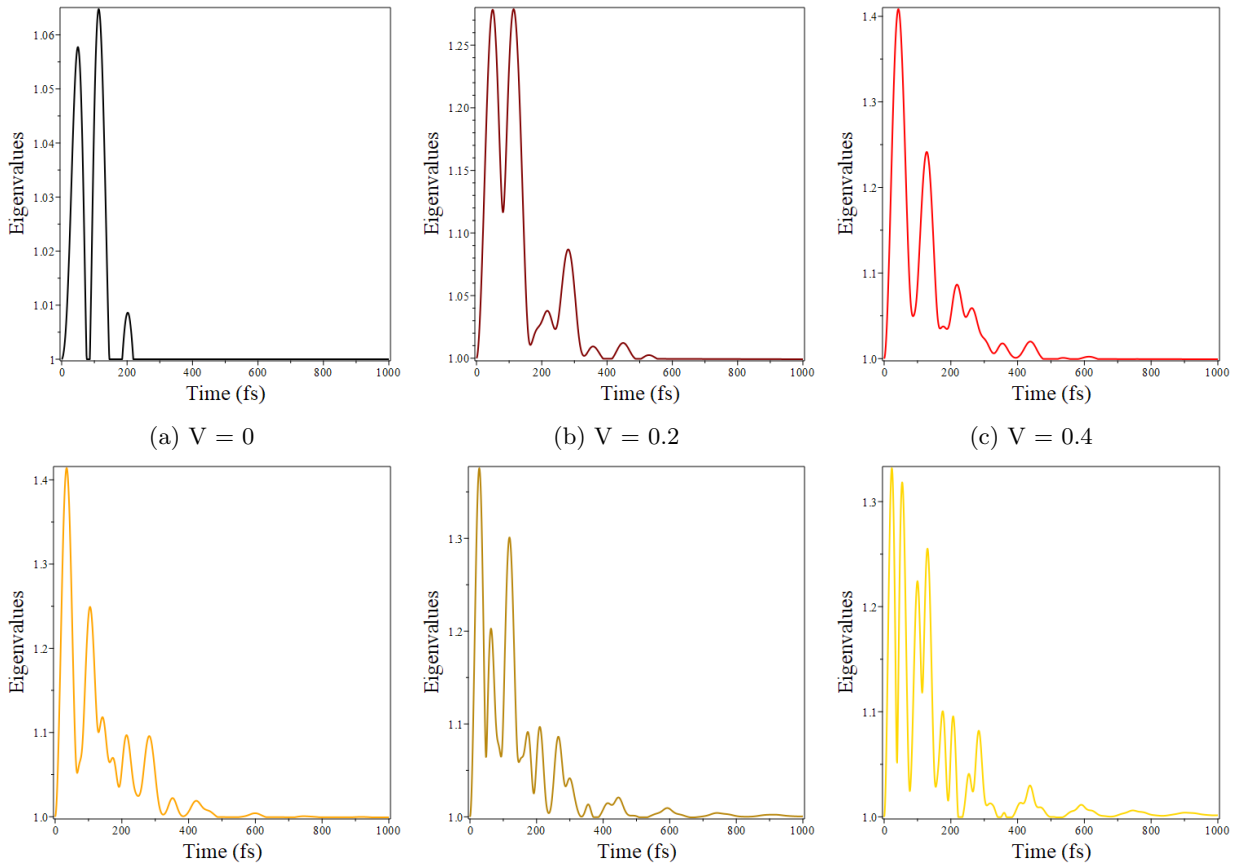

(a) V = 0 (b) V = 0.2 (c) V = 0.4

(d) V = 0.6 (e) V = 0.8 (f) V = 1

FIG. S14: λ_G Dynamics for localized model with two sites per chromophore.

IX. ADDITIONAL λ_G DYNAMICS

Fig. S15 shows spectra of the λ_G dynamics for six and ten sites per chromophore for the localized model with $V = 0.6$. Both spectra follow the same patterns described in the main text for increasing the number of sites.

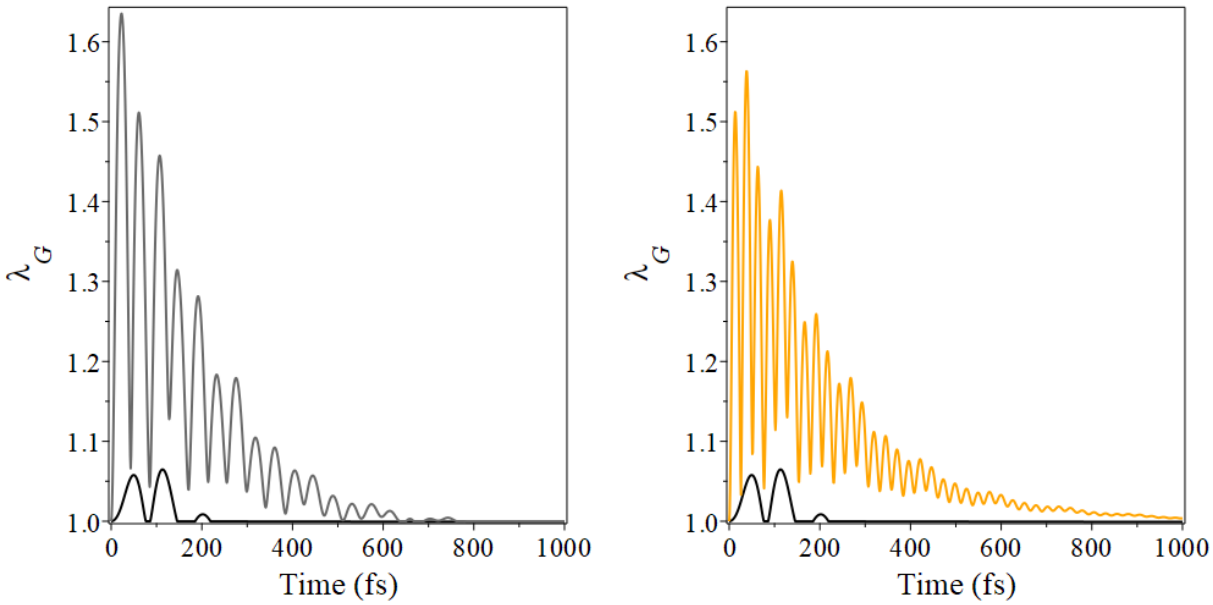

(a) 6 sites per chromophore

(b) 10 sites per chromophore

FIG. S15: λ_G Dynamics for localized model with six and ten sites per chromophore.

X. INTER- VS INTRA-CHROMOPHORE ENTANGLEMENT IN λ_G

Fig. S16 shows the breakdown of the contribution of basis states to the large eigenvalue mode for the entangled and localized models with four and 20 sites per chromphore with $V = 0.6$. In the entangled model, all sites on a specific chromophore are equivalent so each chromphore is represented by a single line and star symbol. Each star represents a peak in the spectrum, demonstrating that peaks in the value of λ_G occur where the contributions from chromophores 1 and 2 approach equality, but the contributions of chromophores 1 and 2 oscillate like the populations. Because the individual sites on the chromphores are equal, it is clear from the spectrum that the peaks result from contributions from a combination of inter- and intra-chromophore entanglement. For the 20 site case, few peaks occur in the first 500 fs of the spectrum because the value of λ_G is so large from the initial intra-chromophore entanglement that the subsequent peaks due to inter-chromophore entanglement are washed out.

The localized case is slightly more complicated, because the contributions from the sites on the individual chromphores are not equivalent. In these spectra, one site corresponding to the excited site in the initial timestep contributes differently to the large eigenvalue mode than all the others. This site is represented by the diamonds and all the other sites (which contribute equally) are represented by squares. As in the entangled model, peaks appear to occur most often in the four site per chromophore case when the contributions are close from chromophores 1 and 2. Moreover, the largest peaks in the spectra occur where the contributions from all sites on those chromphore are close to equal, indicating that the peaks result from a combination of inter- and intra-chromophore entanglement. In the 20 site case, although the excitation site contributions are often quite different from those of the rest of the sites, even for large peaks, given the large number of other sites, those peaks likely still have significant intra-chromophore entanglement. Additionally, peaks occur even when the contributions from chromophores 1 and 2 are not close, meaning some of these peaks are likely primarily the result of intra-chromophore entanglement. The 20 site case also visibly retains the oscillation pattern of the excitation populations, even though the contributions to the large eigenvalue mode are not necessarily directly related to the populations, such that the inter-chromophore entanglement follows this pattern.

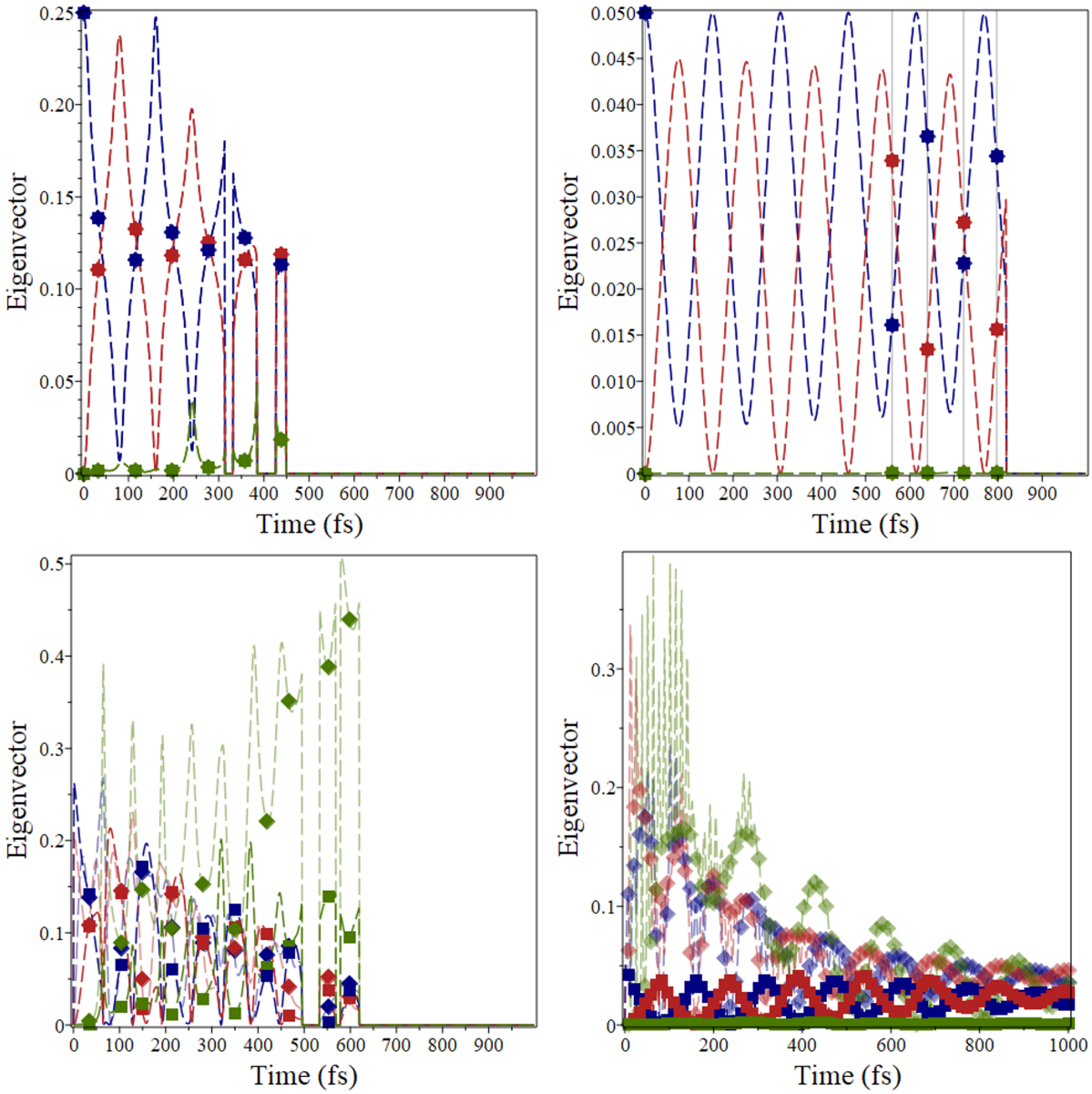

FIG. S16: Breakdown of the inter- and intra-chromophore contributions to the large eigenvalue mode for the: (top) entangled model with (left) four sites per chromophore and (right) 20 sites per chromophore, and (bottom) localized model with (left) four sites per chromophore and (right) 20 sites per chromophore. Symbols appear at the peaks in the spectra and chromophore 1 is blue, chromophore 2 is red, and chromophore 3 is green. In the localized model, the excitation site path is represented by diamond symbols (and the accompanying lines) and the other sites are squares (with the accompanying lines).

[1] Caruso, F.; Chin, A. W.; Datta, A.; Huelga, S. F.; Plenio, M. B. Highly efficient energy excitation transfer in light-harvesting complexes: The fundamental role of noise-assisted transport. *J. Chem. Phys* **2009**, *131*, 105106.
[2] Smart, S. E.; Schuster, D. I.; Mazziotti, D. A. Experimental data from a quantum computer verifies the generalized Pauli exclusion principle. *Communications Physics* **2019**, *2*, 11.
[3] Sager, L. M.; Smart, S. E.; Mazziotti, D. A. Preparation of an exciton condensate of photons on a 53-qubit quantum computer. *Phys. Rev. Res.* **2020**, *2*, 043205.